Available online at www.sciencedirect.com
ScienceDirect
Trans. Nonferrous Met. Soc. China 25(2015) 3232−3239
Transactions of Nonferrous Metals Society of China
www.tnmsc.cn

Hot deformation behavior and processing maps of as-cast Mg−8Zn−1Al−0.5Cu−0.5Mn alloy

Shao-zhen ZHU[1,2], Tian-jiao LUO[2], Ting-an ZHANG[1], Yuan-sheng YANG[2]

1. School of Materials and Metallurgy, Northeastern University, Shenyang 110819, China;
2. Institute of Metal Research, Chinese Academy of Science, Shenyang 110016, China

Received 9 December 2014; accepted 15 April 2015

Abstract: The hot deformation behavior of as-cast Mg−8Zn−1Al−0.5Cu−0.5Mn alloy was studied by hot compression tests at temperatures of 200−350 °C and strain rates of 0.001−1 s^{-1}. The results show that the flow stress increases significantly with increasing strain rate, and decreases as the temperature increases. The flow stress model based on the regression analysis was developed to predict the flow behavior of Mg−8Zn−1Al−0.5Cu−0.5Mn alloy during the hot compression, and the model shows a good agreement with experimental results. Meanwhile, the processing maps were established according to the dynamic materials model. The processing maps show that the increase of strain enlarges the instability domains, and the alloy shows good hot workability at high temperatures and low strain rates.

Key words: magnesium alloy; hot deformation; flow stress; processing map; dynamic recrystallization

1 Introduction

Magnesium alloys are attracting much attention in automotive, aerospace, and 3C industries because of their low density, good castability, high specific strength and specific stiffness, etc [1,2]. A majority of the magnesium components are fabricated by die-casting, gravity casting, low-pressure casting, etc [1]. However, the mechanical properties of components fabricated by casting technologies are low due to their coarse grains and casting defects, which affect the population of magnesium alloys greatly. Recently, wrought magnesium alloys have gotten increasing attention on account of their excellent mechanical properties [3]. However, the workability of magnesium alloys is poor at room temperature due to their hexagonal closed-packed crystal structure and the limited number of slip systems. It is generally known that the workability of magnesium alloys increases at elevated temperatures because of the activation of the non-basal plane [4]. As a result, warm or hot forming processes such as extrusion, forging, and rolling are used as the effective ways for the manufacture of wrought magnesium alloys components [5,6]. Therefore, it is necessary to study the workability and microstructure evolution of magnesium alloys by hot compression tests [7].

It is well known that the Mg−Zn series alloys have great potential for the development of the alloys used for elevated temperature applications due to the thermal stability of Mg−Zn phase [8]. Meanwhile, Mg−Zn series alloys are age-hardenable, so it is possible to improve the tensile strength by heat treatment [9]. Whereas, Mg−Zn alloys have coarse grains and are more sensitive to hot tearing. It is generally accepted that micro-alloying can significantly improve the properties of magnesium alloy [10]. Alloying with expensive elements, such as Zr, RE and Ag, can improve mechanical properties of magnesium alloys, but the cost also increases at the same time. Recently, a high strength Mg−8Zn−1Al−0.5Cu−0.5Mn (mass fraction, %) alloy with outstanding ductility and high strength has been developed in as-cast condition [11]. The addition of Al and Cu can not only accelerate the age-hardening process and increase the density of precipitates but also improve the castability of magnesium alloys [12−14]. So, Mg−8Zn−1Al−0.5Cu−0.5Mn alloy is likely to be developed into a new wrought magnesium alloy with comprehensive mechanical

Foundation item: Project (51274184) supported by the National Natural Science Foundation of China; Project (2013CB632205) supported by the National Basic Research Program of China
Corresponding author: Yuan-sheng YANG; Tel: +86-24-23971728; E-mail: ysyang@imr.ac.cn
DOI: 10.1016/S1003-6326(15)63957-7

properties and reasonable cost, but there is a lack of study on its workability now. Therefore, the aim of this study is to study the hot deformation behavior of the alloy by hot compression tests so as to realize its hot workability and obtain the processing maps from the experimental data. With the guidance of the processing maps, it is possible to optimize the processing parameters in the hot working process, thereby saving time and cost in the future work.

2 Experimental

The as-cast Mg−8Zn−1Al−0.5Cu−0.5Mn magnesium alloy (named as ZACM8100) ingots were prepared by gravity casting and then were machined into cylindrical specimens with 8 mm in diameter and 12 mm in height. The specimens were homogenized at 365 °C for 60 h. Then, the compression tests were conducted on a Gleeble 3800 thermal simulator testing machine at temperatures of 250−350 °C and strain rates of 0.001−1 s^{-1}. The temperatures were measured and controlled by the thermocouples welded at the half-height of the specimen. The specimens were heated to deformation temperature at the rate of 5 °C/s, held at the temperature for 5 min, and then deformed with the height reduction of 60%. All the specimens were quenched in water immediately after the deformation in order to retain the deformed microstructures.

The deformed specimens were cut parallel to the compression axis for microstructure observation. Samples for optical microscopy (OM) observation and SEM were etched in a solution of 4.2 g picric acid + 10 mL water + 10 mL acetic acid + 70 mL ethanol after mechanical polishing.

3 Results and discussion

3.1 Flow stress behavior

The true stress−strain curves of ZACM8100 magnesium alloy compressed at different temperatures and various strain rates are shown in Fig. 1.

As can be seen from the curves, the flow stress increases as the true strain increases and then reaches a maximum, at last decreases to a steady state and this result is the typical characteristic of dynamic recrystallization (DRX) in hot working process [15]. During the initial stage of hot deformation, the quick multiplication of dislocations results in work hardening effect as the strain increases. Then, the DRX occurs when the strain reaches a critical value, which will counteract the effect of work hardening. With the continuing increase of strain, more and more dislocations

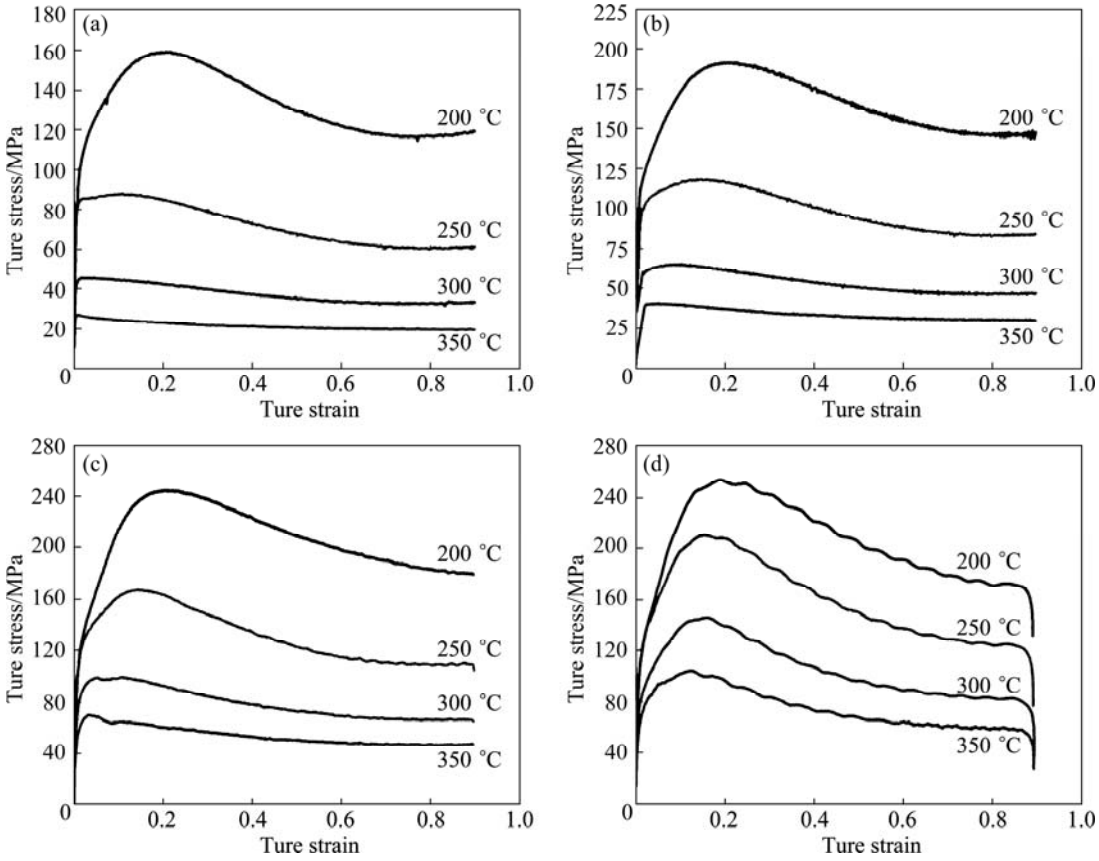

Fig. 1 True stress−strain curves at different deformation temperatures and different strain rates: (a) 0.001 s^{-1}; (b) 0.01 s^{-1}; (c) 0.1 s^{-1}; (d) 1 s^{-1}

are annihilated due to the DRX, which leads to the decrease of flow stress. Eventually, the flow stress decreases to a steady state when the balance is reached between the work hardening and the softening effect caused by DRX.

Meanwhile, it can be seen that the flow stress increases significantly with increasing strain rate. This is because the increment of strain rate will cause higher dislocation density at grain boundaries so as to weaken the softening effect caused by DRX [16]. In contrast, the flow stress decreases as the temperature increases when the strain rate is fixed, which is attributed to two reasons: 1) higher temperature can provide higher mobility of grain boundaries, which benefits the nucleation of DRX, and thus accelerating the process of dislocation annihilation [17]; 2) the critical resolved shear stress (CRSS) for non-basal slip systems decreases with increasing temperature.

3.2 Constitutive equation

The relationship among flow stress, strain rate and temperature can be described by three different constitutive equations [18]. At low stress level, the relationship among flow stress, strain rate and temperature can be described by the exponential law:

$$\dot{\varepsilon} = A_1\sigma^{n_1}\exp[Q/(RT)] \quad (1)$$

At high stress level, the relationship among flow stress, strain rate and temperature can be described by the power exponential law:

$$\dot{\varepsilon} = A_2\exp(\beta\sigma)[-Q/(RT)] \quad (2)$$

At all stress levels, the relationship among flow stress, strain rate and temperature can be described by the hyperbolic sine law:

$$\dot{\varepsilon} = A[\sinh(\alpha\sigma)]^n\exp[-Q/(RT)] \quad (3)$$

where $\dot{\varepsilon}$ is the strain rate; Q is the activation energy for deformation; R is the molar gas constant; T is the thermodynamic temperature; A_1, A_2, A, n_1, n, α and β are material constants.

It is generally accepted to use the hyperbolic sine law to describe the interaction relationship among peak stress, temperature and strain rate. By taking natural logarithm on both sides of Eqs. (1)−(3), the equations can be written as follows:

$$\ln\dot{\varepsilon} = \ln A_1 + n_1\ln\sigma_p - Q/(RT) \quad (4)$$

$$\ln\dot{\varepsilon} = \ln A_2 + \beta\sigma_p - Q/(RT) \quad (5)$$

$$\ln\dot{\varepsilon} = \ln A + n\ln[\sinh(\alpha\sigma_p)] - Q/(RT) \quad (6)$$

According to Eqs. (4) and (5), $n_1 = \mathrm{d}\ln\dot{\varepsilon}/\mathrm{d}\ln\sigma_p$, $\beta = \mathrm{d}\ln\dot{\varepsilon}/\mathrm{d}\sigma_p$. The mean value of n_1 and β can be determined from the slopes of $\ln\sigma_p - \ln\dot{\varepsilon}$ (Fig. 2(a)) and $\sigma_p - \ln\dot{\varepsilon}$ (Fig. 2(b)), therefore, n_1=8.198, β=0.071 MPa^{-1}, $\alpha=\beta/n_1$=0.00866 MPa^{-1}.

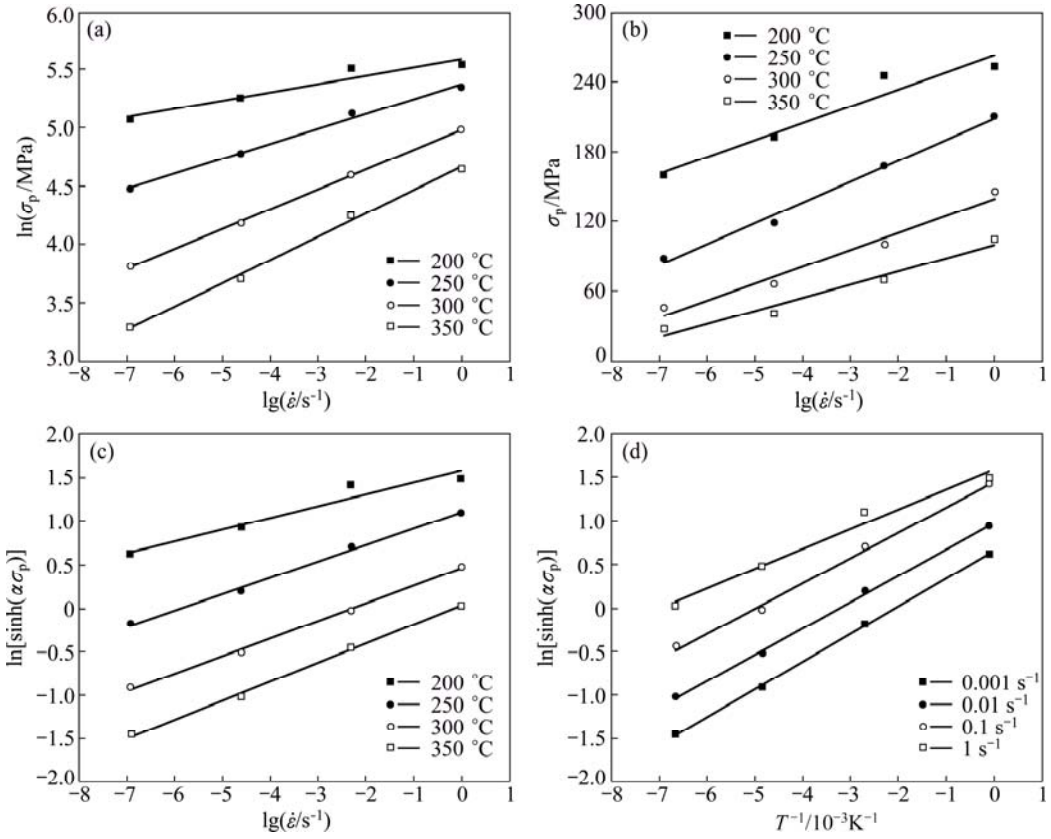

Fig. 2 Relationships among peak stress, strain rate and temperature: (a) $\ln\sigma_p - \ln\dot{\varepsilon}$; (b) $\sigma_p - \ln\dot{\varepsilon}$; (c) $\ln[\sinh(\alpha\sigma_p)] - \ln\dot{\varepsilon}$; (d) $\ln[\sinh(\alpha\sigma_p)] - T^{-1}$

Based on Eq. (6), when the strain rate is fixed, the hot deformation activation energy Q can be expressed as

$$Q = R\left\{\frac{\partial \ln \dot{\varepsilon}}{\partial \ln[\sinh(\alpha\sigma_p)]}\right\}_T \left\{\frac{\partial \ln[\sinh(\alpha\sigma_p)]}{\partial(1/T)}\right\}_{\dot{\varepsilon}} \quad (7)$$

The mean value of Q can be obtained by substituting the slops of Figs. 2(c) and (d) into Eq. (7), and it is 170 kJ/mol. The stress exponent n is determined as 5.606 from the slopes of $\ln[\sinh(\alpha\sigma_p)] - \ln\dot{\varepsilon}$ (Fig. 2(c)).

The combined effects of the temperature and strain rate on deformation behavior can be expressed by the Zener−Hollomon parameter [18,19]:

$$Z = \dot{\varepsilon}\exp[Q/(RT)] = A[\sinh(\alpha\sigma_p)]^n \quad (8)$$

By taking natural logarithm on both sides of Eq. (8), the equations can be written as follows:

$$\ln Z = \ln A + n\ln[\sinh(\alpha\sigma_p)] \quad (9)$$

The liner relationship between Z and $\ln[\sinh(\alpha\sigma_p)]$ is shown in Fig. 3. The regression coefficient is 0.98. The intercept of fitted line in Fig. 3 is equal to the value of $\ln A$, and the value of A is calculated as 3.20×10^{14}.

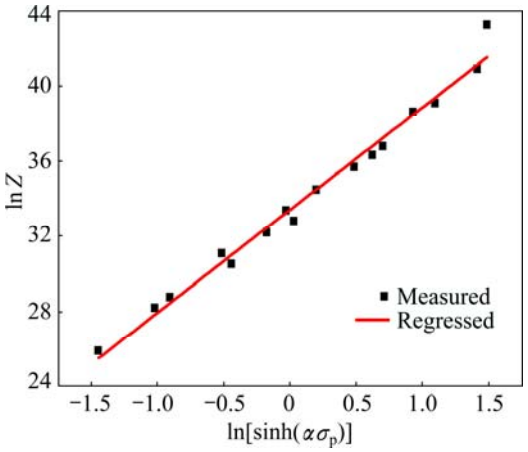

Fig. 3 Relationship between Z and $\ln[\sinh(\alpha\sigma_p)]$

Substituting the values of α, Q, n and A into Eq. (3), the constitutive equation of ZACM8100 alloy can be written as

$$\dot{\varepsilon} = 3.20\times10^{14}\left[\sinh(0.0086\sigma_p)\right]^{5.606}\cdot \exp[-1.70\times10^5/(RT)] \quad (10)$$

3.3 Modeling of flow stress

The constitutive equation is established on a theoretical basis of creep model [20], and thus the peak stress is taken into account in constitutive equation generally. However, the peak stress cannot stand for the flow stress behavior during the hot compression process. In order to accurately describe the flow stress behavior of the alloy in a wide hot deformation range, the modeling of flow stress including strain was established in this work.

Based on the regression analysis, the material constants (α, n, Q, $\ln A$) of constitutive equations can be calculated by using the values of the flow stress under different true strains within the range of 0.05−0.85 at the interval of 0.05. The relationship between material constants and strain can be fitted by quintic polynomial, as shown in Fig. 4. So, the modeling of flow stress can be expressed as

$$\dot{\varepsilon} = A\left[\sinh(\alpha\sigma)\right]^n \exp[-Q/(RT)] \quad (11)$$

where

α=0.00765+0.0102ε−0.04ε^2+0.1727ε^3−0.2484ε^4+0.1132ε^5,

n=15.11−139.86ε+706.86ε^2−1610.18ε^3+1696.18ε^4−670.25ε^5,

Q=259.26−1591.44ε+9579.75ε^2−23743.46ε^3+26338.46ε^4 − 10788.44ε^5,

$\ln A$=57.65−412.68ε+2426.19ε^2−5990.96ε^3+6646.11ε^4−2724.46ε^5.

In order to verify the flow stress model, the comparisons between the calculated results and experimental results are presented in Fig. 5. It is obviously found that the experimental and calculated results show a good agreement in most cases, except when the strain rate is 1 s^{-1}. Therefore, the flow stress model is an efficient way to predict the flow behavior of ZACM8100 alloy during the hot compression and more detail information about the deformation process can be acquired from it.

3.4 Processing maps

The processing map is based on the dynamic materials model [21]. The work piece is considered to be a dissipater of power in this model, and the efficiency of power dissipation (η) occurring through microstructural changes during hot deformation is given by

$$\eta = 2m/(m+1) \quad (12)$$

where m is the strain rate sensitivity of flow stress given by $\partial(\ln\sigma)/\partial(\ln\dot{\varepsilon})$. The variation of η with deformation temperature and strain rate constitutes the power dissipation map.

Furthermore, in order to identify the regime of flow instability during the deformation, PRASAD and SEAHACHARYULU [22] developed the instability criterion based on the extremum principles of irreversible thermodynamics as applied to continuum mechanics of large plastic flow, flow instability will occur if

$$\xi(\dot{\varepsilon}) = \frac{\partial \ln\left[m/(m+1)\right]}{\partial \ln\dot{\varepsilon}} + m \le 0 \quad (13)$$

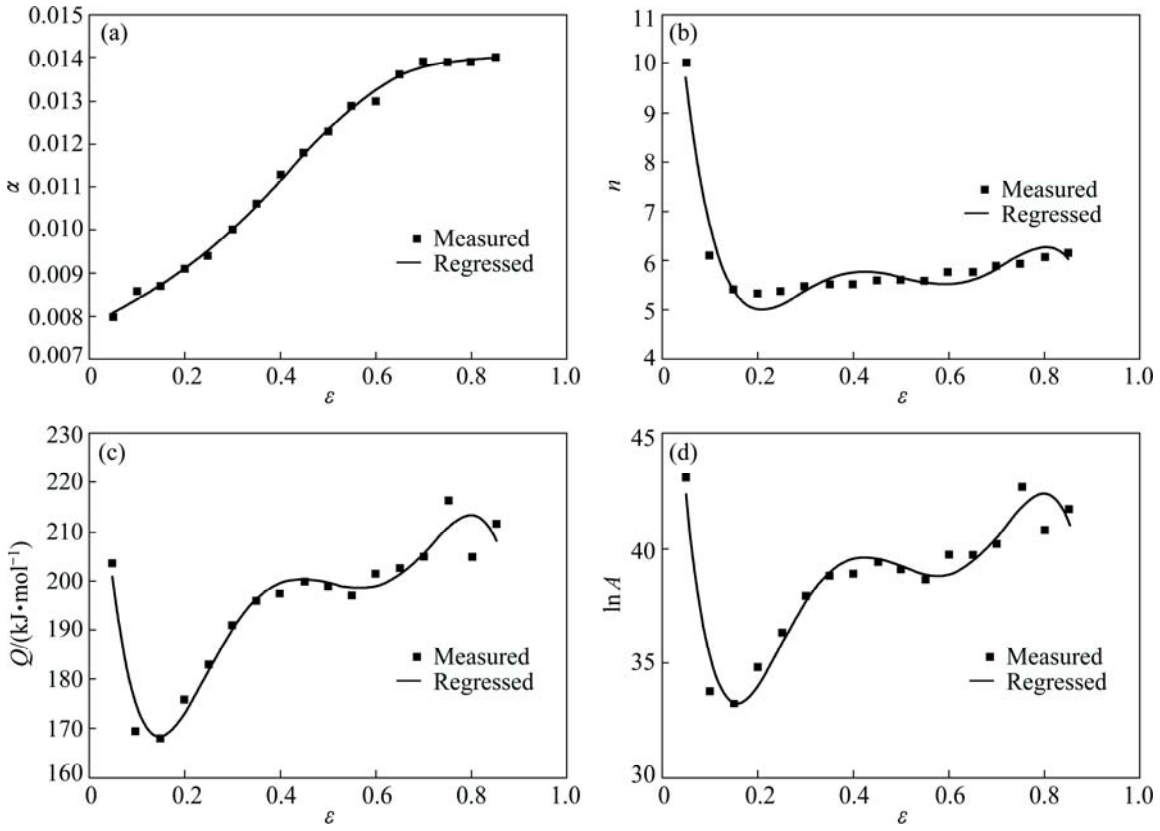

Fig. 4 Relationships between material constants and strain: (a) α–ε; (b) n–ε; (c) Q–ε; (d) ln A–ε

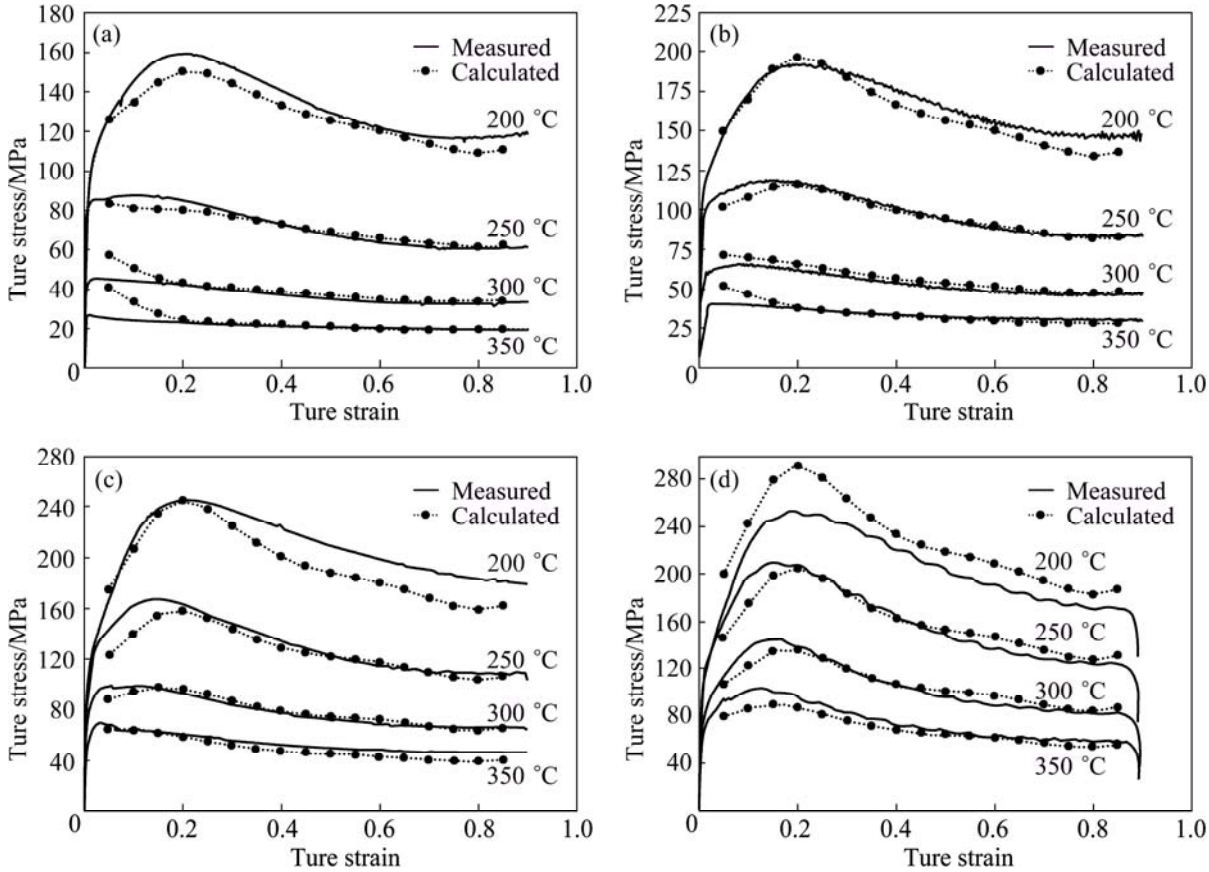

Fig. 5 Comparisons between experimental and predicted flow stress at different deformation temperatures and different strain rates: (a) 0.001 s^{-1}; (b) 0.01 s^{-1}; (c) 0.1 s^{-1}; (d) 1 s^{-1}

The instability map can be obtained by representing the variations of $\xi(\dot{\varepsilon})$ with deformation temperatures and strain rates, and then it is overlaid onto the power dissipation map to obtain the processing map.

The processing maps obtained at strains of 0.1, 0.3, 0.5, 0.85 are shown in Fig. 6. Different colors represent the efficiency of power dissipation and the shaded areas represent the regimes of flow instability.

From Fig. 6, it can be found that the processing maps have a close relationship with the strain and the increase of strain enlarges the instability domains.

It is widely accepted that the efficiency values corresponding to the dynamic recrystallization are about 0.3−0.4 [22,23]. The domains where complete DRX occurs with the efficiency of power dissipation higher than 0.3 are shown in Fig. 6.

At the strain of 0.1, domain I occurs in the temperature range of 312−350 °C and the strain rate range of 0.001−0.22 s^{-1}, with a peak efficiency of about 0.375 corresponding to 350 °C and 0.001 s^{-1}.

At the strain of 0.3, domain II occurs in the temperature range of 308−350 °C and the strain rate range of 0.001−0.37 s^{-1}, with a peak efficiency of about 0.35 corresponding to 350 °C and 0.02 s^{-1}.

At the strain of 0.5, domain III occurs in the temperature range of 318−350 °C and the strain rate range of 0.001−0.08 s^{-1}, with a peak efficiency of about 0.325 corresponding to 350 °C and 0.007 s^{-1}.

At the strain of 0.85, domain IV occurs in the temperature range of 318−350 °C and the strain rate range of 0.001−0.05 s^{-1}, with a peak efficiency of about 0.325 corresponding to 350 °C and 0.01 s^{-1}.

The domains are optimal parameters for hot working process of the ZACM8100 magnesium alloy, according to the above analyses, the ZACM8100 magnesium alloy shows good hot workability at high temperatures and low strain rates under different strain conditions.

3.5 Microstructure analysis

The microstructures of ZACM8100 alloy compressed at a strain rate of 0.1 s^{-1} and different temperatures are shown in Fig. 7. It is clearly found that the area fraction and the size of the recrystallized grains increase along with the increasing temperatures. When the deformation temperatures are 200 and 250 °C, the "necklace" structure occurs at the initial grain boundary or twins, which means that the DRX is not complete. When the deformation temperature reaches 300 and 350 °C, the homogeneity of the microstructure is gradually increased. However, the driving force of DRX increases with the increasing temperature, as a result, the size of the recrystallized grains is obvious lager than that in the samples deformed at 200 and 250 °C.

Figure 8 shows the effect of the strain rates on the microstructures of ZACM8100 alloy compressed at 250 °C. It can be found that the fine recrystallized grains generate in the most areas. However, the area fraction of the recrystallized grains decreases with the increasing strain rate, and the non-homogeneity of microstructure

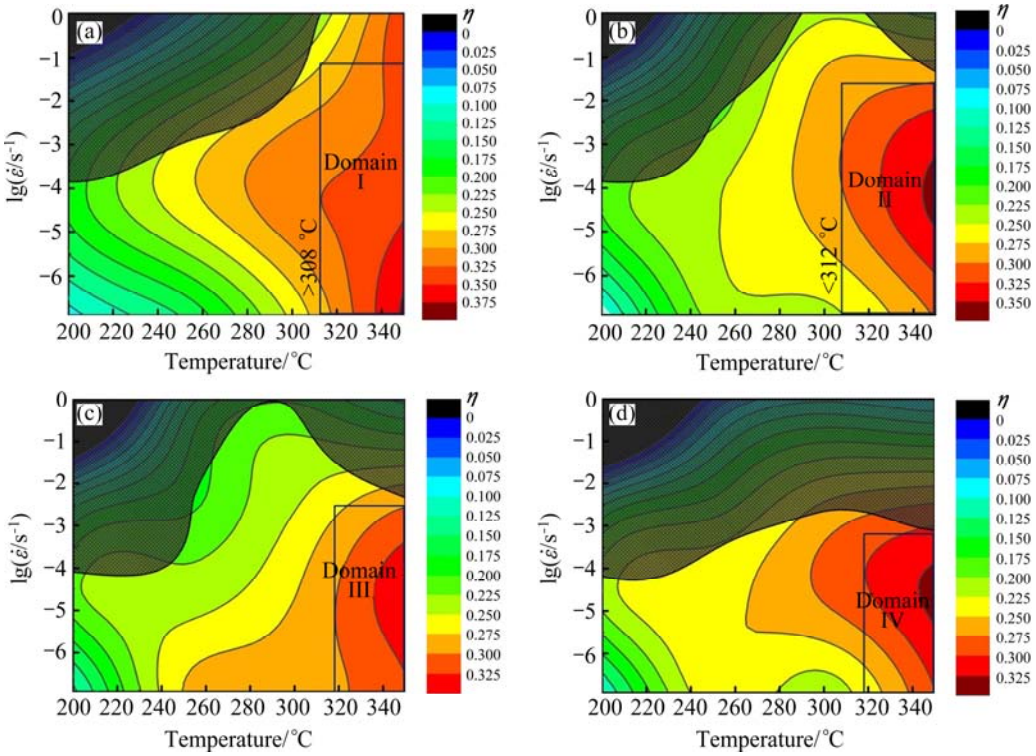

Fig. 6 Processing maps for ZACM8100 magnesium alloy under various strains: (a) ε=0.1; (b) ε=0.3; (c) ε=0.5; (d) ε=0.85

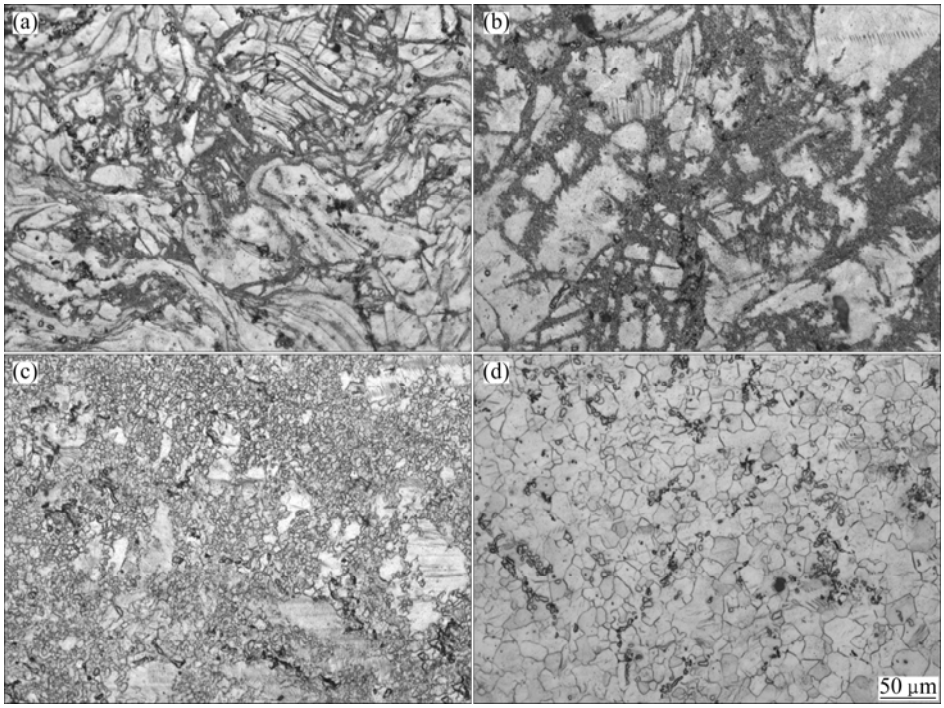

Fig. 7 Optical microstructures of magnesium alloy ZACM8100 hot-compressed at strain rate of 0.1 s^{-1} and various temperatures: (a) 200 °C; (b) 250 °C; (c) 300 °C; (d) 350 °C

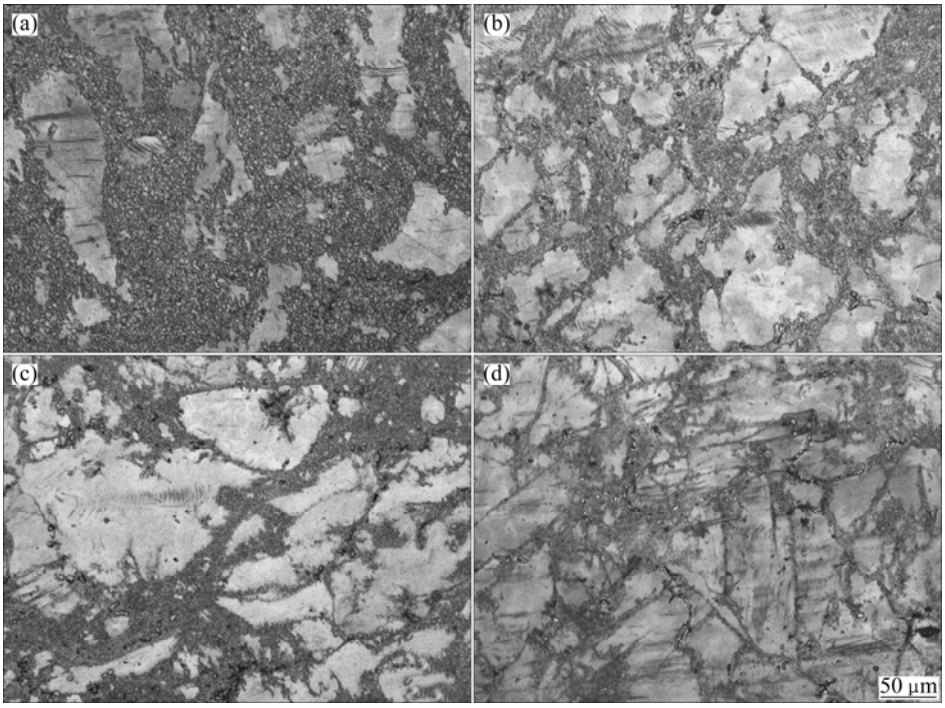

Fig. 8 Optical microstructures of ZACM8100 magnesium alloy hot-compressed at temperatures of 250 °C and various strain rates: (a) 0.001 s^{-1}; (b) 0.01 s^{-1}; (c) 0.1 s^{-1}; (d) 1 s^{-1}

is more obvious. This is because the density of twins increases with the increase of the strain rate, and recrystallized grains formed in twins are the main mechanism of DRX. On the contrary, the recrystallized grains formed at grain boundaries decrease [4].

Considering the above analyses, higher temperature and lower strain rate are beneficial for the recrystallization during hot deformation, and the effect of temperature on the size of the recrystallized grains is more obvious than strain rate. This is because temperature has exponent relation with the Zener−Hollomon parameter and strain rate has linear relation with it according to Eq. (8). So, temperature is the first consideration during the hot forming process.

4 Conclusions

1) The constitutive equation of ZACM8100 alloy for hot deformation is $\dot{\varepsilon}=3.20\times10^{14}\cdot[\sinh(0.0086\sigma_p)]^{5.606}\exp[-1.70\times10^5/(RT)]$.

2) The processing maps have a close relationship with the strain. The increase of strain enlarges the instability domains. The ZACM8100 magnesium alloy shows good hot workability at high temperatures and low strain rates.

3) High temperatures and low strain rates are beneficial for the recrystallization during hot deformation, and the effect of temperature on the size of the recrystallized grains is more obvious than strain rate.

References

[1] LUO A A. Magnesium casting technology for structural applications [J]. Journal of Magnesium and Alloys, 2013, 1(1): 2−22.

[2] FURUYA H, KOGISO N, MATUNAGA S, SENDA K. Application of magnesium alloys for aerospace structure systems [J]. Materials Science Forum, 2000, 350: 341−348.

[3] PAN Fu-sheng, ZHANG Jing, WANG Jing-feng, YANG Ming-bo, HAN En-hou, CHEN Rong-shi. Key R&D activities for development of new types of wrought magnesium alloys in China [J]. Transactions of Nonferrous Metals Society of China, 2010, 20(7): 1249−1258.

[4] BETTLE C, BARNETT M. Advances in wrought magnesium alloys: Fundamentals of processing, properties and applications [M]. Cambridge: Woodhead Publishing Limited, 72−75.

[5] QUAN G Z, KU T W, SONG W J, KANG B S. The workability evaluation of wrought AZ80 magnesium alloy in hot compression [J]. Materials & Design, 2011, 32(4): 2462−2468.

[6] MIRANDA R. Advances in wrought magnesium alloys [J]. International Journal of Environmental Studies, 2013, 70(2): 336.

[7] LV Bin-jiang, PENG Jian, WANG Yong-jian, AN Xiao-qin, ZHONG Li-ping, TANG Ai-tao, PAN Fu-sheng. Dynamic recrystallization behavior and hot workability of Mg−2.0Zn−0.3Zr−0.9Y alloy by using hot compression test [J]. Materials & Design, 2014, 53: 357−365.

[8] ZHANG Zhan, COUTURE A, LUO A. An investigation of the properties of Mg−Zn−Al alloys [J]. Scripta Materialia, 1998, 39(1): 45−53.

[9] YANG Z, LI J P, ZHANG J X, LORIMER G W, ROBOSON J. Review on research and development of magnesium alloys [J]. Acta Metallurgica Sinica, 2008, 21(5): 313−328.

[10] ALI Y, QIU Dong, JIANG Bin, PAN Fu-sheng, ZHANG Ming-xing. Current research progress in grain refinement of cast magnesium alloys: A review article [J]. Journal of Alloys and Compounds, 2015, 619: 639−651.

[11] WANG Jing, LIU Rui-dong, LUO Tian-jiao, YANG Yuan-sheng. A high strength and ductility Mg−Zn−Al−Cu−Mn magnesium alloy [J]. Materials & Design, 2013, 47: 746−749.

[12] OH-ISHI K, HONO K, SHIN K S. Effect of pre-aging and Al addition on age-hardening and microstructure in Mg−6wt% Zn alloys [J]. Materials Science and Engineering: A, 2008, 496(1): 425−433.

[13] BUHA J, OHKUBO T. Natural aging in Mg−Zn(−Cu) alloys [J]. Metallurgical and Materials Transactions A, 2008, 39(9): 2259−2273.

[14] FOERSTER G S. New developments in Mg die casting [C]//Proceeding of the IMA 33rd Annual Meeting. Dayton: International Magnesium Association, 1976: 35−39.

[15] SAKAI T, JONAS J J. Dynamic recrystallization: Mechanical and microstructural considerations [J]. Acta Metallurgica, 1984, 32(2): 189−209.

[16] WANG Jing, SHI Bao-ling, YANG Yuan-sheng. Hot compression behavior and processing map of cast Mg−4Al−2Sn−Y−Nd alloy [J]. Transactions of Nonferrous Metals Society of China, 2014, 24(3): 626−631.

[17] MA Ming-long, HE Lan-qian, LI Xing-gang, ZHANG Kui. Hot workability of Mg−9Y−1MM−0.6Zr alloy [J]. Journal of Rare Earths, 2011, 29(5): 460−465.

[18] ZENER C, HOLLOMON J H. Effect of strain rate upon plastic flow of steel [J]. Journal of Applied Physics, 1944, 15(1): 22−32.

[19] ZHOU H, WANG Q D, YE B, GUO W. Hot deformation and processing maps of as-extruded Mg−9.8Gd−2.7Y−0.4Zr Mg alloy [J]. Materials Science and Engineering A, 2013, 576: 101−107.

[20] MCQUEEN H J, JONAS J J. Recent advances in hot working: Fundamental dynamic softening mechanism [J]. Journal of Applied Metalworking, 1984, 3(3): 233−241.

[21] PRASAD Y. Processing maps: A status report [J]. Journal of Materials Engineering and Performance, 2003, 12(6): 638−645.

[22] PRASAD Y, SEAHACHARYULU T. Modeling of hot deformation for microstructural control [J]. International Materials Reviews, 1998, 43(6): 243−258.

[23] LV Bing-jiang, PENG Jian, SHI Da-wei, TANG Ai-tao, PAN Fu-sheng. Constitutive modeling of dynamic recrystallization kinetics and processing maps of Mg−2.0Zn−0.3Zr alloy based on true stress–strain curves [J]. Materials Science and Engineering A, 2013, 560: 727−733.

铸态 Mg−8Zn−1Al−0.5Cu−0.5Mn 镁合金的热变形行为和热加工图

朱绍珍[1,2]，罗天骄[2]，张廷安[1]，杨院生[2]

1. 东北大学 材料与冶金学院，沈阳 110819；2. 中国科学院 金属研究所，沈阳 110016

摘 要：采用热压缩实验研究 Mg−8Zn−1Al−0.5Cu−0.5Mn 镁合金在温度为 200~350 °C、应变速率为 0.001~1 s^{-1} 条件下的热变形行为。结果表明，流变应力随着应变速率的增加而明显增大，随着变形温度的升高而减小。同时，采用回归分析的方法建立预测合金流变应力的模型，该模型与实验结果能较好地吻合。以动态材料模型为基础建立合金的热加工图，从加工图中可以看出，随着应变的增大，合金的非稳态区域变大，合金在高温和低应变速率下具有良好的加工性。

关键词：镁合金；热变形行为；流变应力；热加工图；动态再结晶

(Edited by Xiang-qun LI)